Journal of Alloys and Metallurgical Systems 7 (2024) 100086

Contents lists available at ScienceDirect

Journal of Alloys and Metallurgical Systems

journal homepage: www.journals.elsevier.com/journal-of-alloys-and-metallurgical-systems

Hot deformation characteristics and processing map analysis of Al-Zn/ stainless steel particles-based composite

Theo Oluwasegun Joshua [a,b], Kenneth Kanayo Alaneme [a,c,*], Sodiq Abiodun Kareem [a], Michael Oluwatosin Bodunrin [d]

[a] *Materials Design and Structural Integrity Group, Department of Metallurgical and Materials Engineering, Federal University of Technology Akure, P.M.B. 704, Ondo State, Nigeria*

[b] *Department of Metallurgical & Materials Engineering, School of Engineering, Kogi State Polytechnic Itakpe Campus, PMB, 1101, Nigeria*

[c] *Centre for Nanoengineering and Tribocorrosion, School of Mining, Metallurgy and Chemical Engineering, Faculty of Engineering & the Built Environment, University of Johannesburg, South Africa*

[d] *School of Chemical and Metallurgical Engineering and DSI-NRF Centre of Excellence in Strong Materials: All University of the Witwatersrand, Private Bag 3, WITS, Johannesburg 2050, South Africa*

ARTICLE INFO

Keywords:
Al-Zn/6 wt% SSp
Aluminum-based composites
Hot compression
Flow stress
Processing map
Microstructure

ABSTRACT

The hot deformation behavior of Al-Zn/martensitic stainless steel particles-based composite (Al-Zn/6 %SSp), was examined in this study. The composite was tested using isothermal compression at 200–350 °C/0.01–10 s^{-1} and a global strain of 0.5. From the results, it was noticed that the composite's flow stress increased with strain rate increase and drop in temperature. The constitutive equation from the hot-worked composites resulted in an estimated activation energy of 226.27 kJ/mol, which was 58 % more than that for the self-diffusion of aluminum alloy (142 kJ/mol). These findings suggest dynamic recrystallization (DRX) as the dominant deformation mechanism, as confirmed from the microstructures of the hot worked samples mostly at high temperatures and strain rates. Work hardening was predicted to dominate the deformation process by the stress exponent *(n)* value of 10.36 (which exceeded 5), but this was inconsistent with the microstructural observations. Comparing the linear fitting of calculated flow stress data with the estimated flow stress yielded a correlation coefficient (R^2) of approximately 0.97. This observation demonstrates an effective relationship involving the calculated stress with the computed stress value for the composite material that was fabricated. Based on the processing map analysis, the instability regime occurs at 200—270 °C/0.01–10 s^{-1}. The stable domain established was at 280–340°C/ 0.01–10 s^{-1} which is most suitable for achieving the best microstructural conditions for enhanced service performance.

1. Introduction

Aluminum matrix composites (AMCs) reinforced with metallic materials are nascent AMC systems touted to offer enhanced product safety and damage tolerance for load-bearing and structural applications [1]. The improved product reliability had been hinged on the improved ductility and toughness they possess in comparison to conventionally utilized ceramic reinforcement [2]. Thus, there seems to be a growing interest in understanding the full spectra of mechanical and material behavior exhibited by metallic material-reinforced AMCs [3]. In several studies that have been carried out using metals such as Ni, Mo, Ti, Cu, Fe, and martensitic stainless steel; matrix refinement, size and shape of particle grains, enhanced interface strengthening, and dislocation density are some of the mechanisms on display, responsible for the enhanced mechanical properties of the AMCs [1–4]. However, Alaneme *et al.* [2] already noted that warm temperature and hot temperature working may be essential for the more productive and successful development of intricately shaped parts and components with the use of AMCs developed with metallic reinforcements.

Metal deformation at high temperatures has given metal fabricators the privilege of lowering the deformation load, altering microstructure, and controlling the final material characteristics while ensuring that production costs are as minimal as possible [5]. Huang, [6] in his work indicated that the preference of the best hot working process parameters

* Corresponding author at: Materials Design and Structural Integrity Group, Department of Metallurgical and Materials Engineering, Federal University of Technology Akure, P.M.B. 704, Ondo State, Nigeria.

https://doi.org/10.1016/j.jalmes.2024.100086
Received 22 April 2024; Received in revised form 22 May 2024; Accepted 11 June 2024
Available online 13 June 2024

is more often than not controlled by the information available on the flow behavior of the AMCs, nature of reinforcement, amount of reinforcement added, deformation parameters, and preliminary microstructure among others.

Furthermore, the plastic flow characteristics of metals and alloys and their responses under high temperatures and prevailing loading conditions are usually determined by constitutive relations. The use of constitutive equations in determining the flow stress of a hot deformed metal has been reported to yield accurate indicators important in implementing specific metal-forming processes from mechanical to metallurgical standpoints [7]. Constitutive models serve the purpose of accurately predicting flow stress data, as well as determining the stress exponents and the activation energy. These parameters are valuable for accurately predicting the underlying deformation mechanism in a specific deformation process and assessing the hot workability of the composite material [8,9]. Processing maps are used to express the hot workability of metallic materials and explain the possible conditions for forming material at varying temperatures, strain rates, and strain. It suggests the influence of previous processing and the initial microstructure of the material on the hot workability. It is a tool used to assess deformation mechanisms and optimize the process parameters of materials, which is a valuable tool to guarantee a flaw-free final product [10–13].

Alaneme et al. [14] employed a constitutive equation to investigate the hot deformation characteristics of AA6063-based composites containing Ni and Steel particles as reinforcements. The investigation was conducted at temperatures of 200–400 °C/0.01–10 s^{-1}, respectively. It was observed that work hardening by particle-dispersion hardening, was the dominant deformation mechanism. Babalola et al. [8] investigated hot compression and microstructural analysis of aluminum-matrix composites containing Ni and SiC particles. The findings indicate that the flow stress experienced in the AMCs was greatly affected by the deformation conditions imposed and the reinforcement types employed. Nickel powder-reinforced AMC shows superior resistance to deformation to that of silicon carbide-reinforced AMC across various testing settings. The hot deformation studies of aluminium-matrix composite reinforced with Ni particles was undertaken by Alaneme et al. [1]. The hot compression test was conducted at the temperatures and strain rates of 200–400 °C/0.01–10 s^{-1}. The findings indicate that the Al6063/Nip composite exhibited maximal power dissipation efficiencies within 390 – 400 °C/0.01 s^{-1} and 260 – 350 °C/10 s^{-1}, thereby establishing the safe processing windows. Dynamic recrystallization and dynamic recovery were identified as the primary mechanisms for flow softening in the lower and higher domains, respectively. Wei et al. [15], using constitutive equations analyzed the hot deformation characteristics of Al-Mg-Si-Cu-Zn alloy under conditions of 350–500 °C/0.01–10 s^{-1}. They obtained 256 kJ/mol^{-1} as the activation energy for the developed alloy and established dynamic recrystallization as the primary mechanism responsible for the softening process.

The above literature survey provides valuable insights on the potential of hot deformation to optimize the microstructure and enhance the mechanical characteristics of aluminium-based composites. However, hardly can related works of literature be sourced for aluminum-based composite reinforced with 6 wt% martensitic stainless steel 410 L, which is the focus of this study. The objective is to analyze how the deformation parameters influence the hot workability of the Al-Zn/ 6 %SSp composite and to develop a constitutive equation using the Arrhenius equation for the calculation of flow stress and deformation mechanism. The findings of this research will be valuable in understanding mechanical working conditions most applicable for development of Al-Zn/6 %SSp composite-based products for industrial and technological use. Due to its exceptional strength, corrosion resistance, wear resistance, rapid work hardening rate, high ductility and toughness, and comparatively low thermal coefficient of expansion compared to other metallic materials, martensitic stainless steel has emerged as a preferred reinforcement material [4,16,17].

2. Materials and method

2.1. Materials

The investigated composite was Al-Zn alloy (composite matrix with chemical composition presented in Table 1) with 6 wt% martensitic stainless steel (45 µm particle size) (Al-Zn 6 wt% SSp). The composite fabrication process adhered to the double stir casting techniques described in Alaneme et al.'s work [18]. In which charge calculation was used to determine the quantity of Al-Zn and martensitic stainless steel (410 L) powder required to fabricate 6 wt% martensitic stainless steel reinforced Al-Zn based composites. Dampness due to the addition of the reinforcement to the matrix was reduced by preheating the stainless steel particle in an oven at a temperature of 270 °C. Gas fired crucible furnace was used to get the Al-Zn alloy to molten state at a temperature of 700 °C. The melt was made to cool to a moderately solid state at a temperature of about 590 °C before the preheated martensitic stainless steel particulates were charged and stirred manually for 5 minutes. The produced slurry mix was reheated to 720 °C, stirred mechanically for 400 rpm for about 5 minutes and then cast into sand molds.

2.2. Composite hot compression

A Gleeble (3500) thermomechanical simulator was used for the hot compression testing of the Al-Zn6wt%SSp composite. The composite was machined to a cylindrical shape of 10 mm× 15 mm dimension, and compressed to a global strain of 50 %, working with 0.01–10.0 s^{-1} and 200°C-350 °C strain rates and temperatures, respectively. Before conducting the test, the wrapping technique was used [19]. The test samples were subjected to 5°C per second heating until they reached the predetermined deformation temperatures. They were then maintained at this temperature for 180 seconds to get a consistent temperature. Standard procedures to mitigate frictional effects between the samples and the pressure head with the use of graphite foil and nickel paste, was adopted before testing. The specimens were subsequently subjected to compression at the specified strain rate until a compression level of 0.5 (50 %) was achieved. For all test conditions, three repeat hot compression was performed to assure for the reproducibility of the data generated. Hyperbolic-sine Arrhenius constitutive equation was adopted to determine the activation energy and stress exponent calculated from the hot compression stress-strain data. The peak stress was employed to calculate the material constant values, which were then utilized to establish the primary deformation mechanisms for the composite material. The developed processing maps were employed to determine the optimal domains for processing the composite material that was produced.

2.3. Microscopy

The produced composite was subjected to structural analysis using a Scanning Electron Microscopy (SEM) in backscattered electron (BSE) mode. Before conducting microstructural analysis, the samples underwent a process of achieving a standard metallographic surface polish

Table 1
Chemical Composition of Al–Zn based alloy.

S/N	ELEMENT	COMPOSITION
1.	Al	88.17
2.	Si	0.40
3.	Fe	0.50
4.	Mn	0.30
5.	Mg	0.50
6.	Zn	9.08
7.	Cr	0.20
8.	Ti	0.20
9.	Cu	0.65

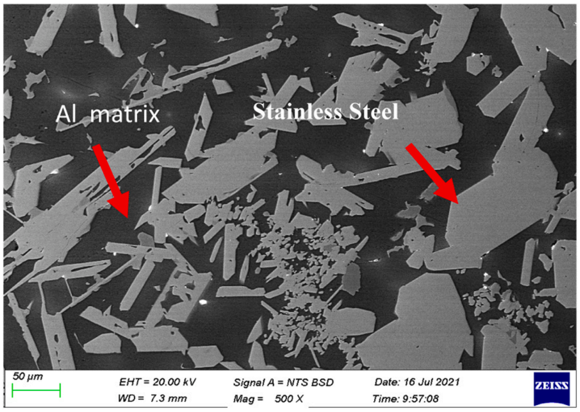

Fig. 1. As-cast microstructure of the Al-Zn/6 % Stainless Steel Particulate composite.

and were subsequently etched with Weck's reagent for 17 seconds. Analysis of the microstructures of deformed samples was subsequently conducted on the center region of the samples, where previous studies have indicated the accumulation of local strain.

3. Results and discussion

3.1. Pre-deformation microstructure

The Scanning Electron Microscopy (SEM) image of the Al-Zn/6 % martensitic stainless steel particles reinforced composite is presented in Fig. 1. The stainless steel particles (light phase) dispersed phase within the Al matrix (dark phase) with signs of particle clustering evident. This is an apparent indication of slightly non-uniform distribution of the particles in the Al-Zn matrix in the as-cast condition, largely due to the significant difference in density between stainless steel and Al-Zn [4].

3.2. Post deformation microstructures

Comparing the as-cast- (Fig. 1) and post-deformation- microstructures (Figs. 2–5, which imaging was taken at the center of the samples where strain localization is most intense during deformation [1]), it was noticed that the hot deformed samples had more refined grain structure and redistributed reinforcement particles. The grain orientations in Fig. 2a–d, which showcases elongated grains along deformation direction, shear bands, and cracks, indicates the accumulation of high dislocations density at 200 °C/0.01–10 s^{-1}. This suggests that work hardening predominates at low temperatures. The features in the microstructures in Fig. 3 also show elongated grains parallel to the deformation axis, and the existence of shear bands, which indicates high prevalence of work hardening at this deformation condition (250 °C/0.01 – 1.0 s^{-1}).

Fig. 4a-c which show the post deformation microstructure of samples processed at 300 °C/0.01–1.0 s^{-1}, indicate the formation of strain-free new grains. Grain distortion as experienced in Figs. 2 and 3 are less pronounced in Fig. 4a–c as the deformation temperature is increased. Fine recrystallized grains were observed around the initial grains, especially in Fig. 4a–c which is due to the relatively higher deformation temperature (300 °C), which provides higher thermal activation for the complete annihilation of dislocations, consequently enhancing DRX

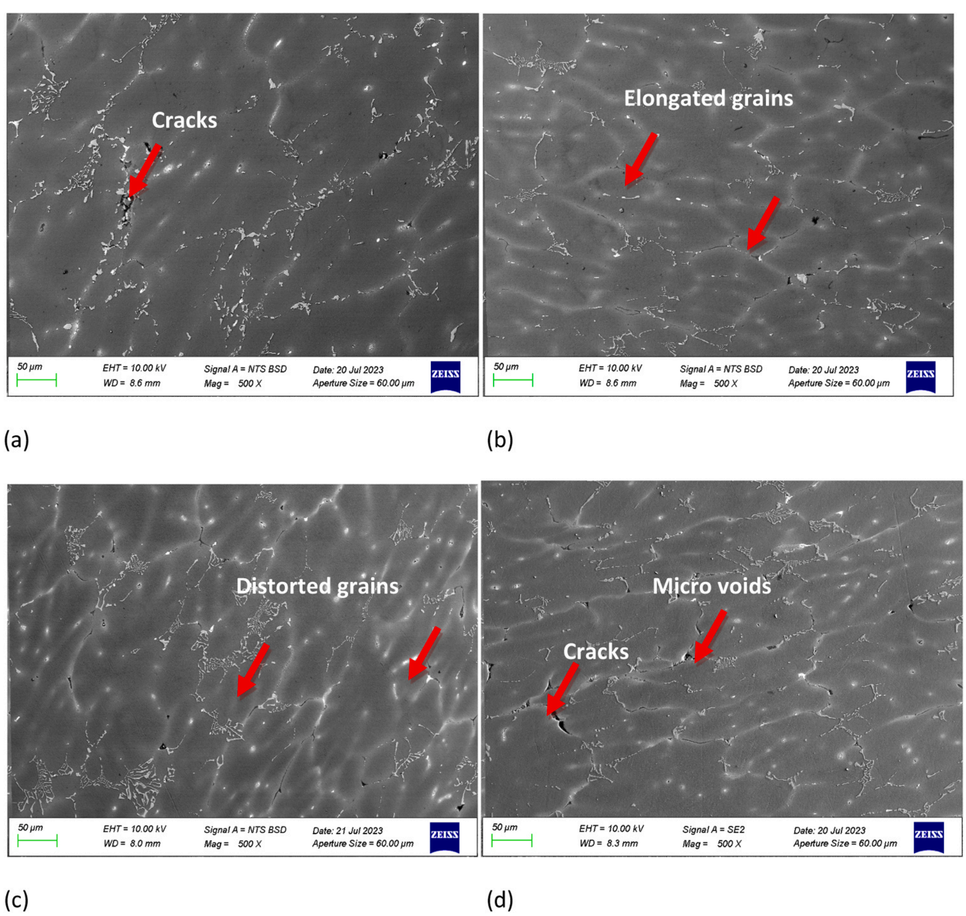

Fig. 2. Representative SEM images of the instability regions at lower temperature of hot-compressed (0.5 global strain) Al-Zn/6 wt%SSp composites at (a) 200 °C /0.01 s^{-1}, (b) 200 °C/0.1 s^{-1}, (c) 200 °C/1.0 s^{-1}, and (d) 200 °C/10.0 s^{-1}.

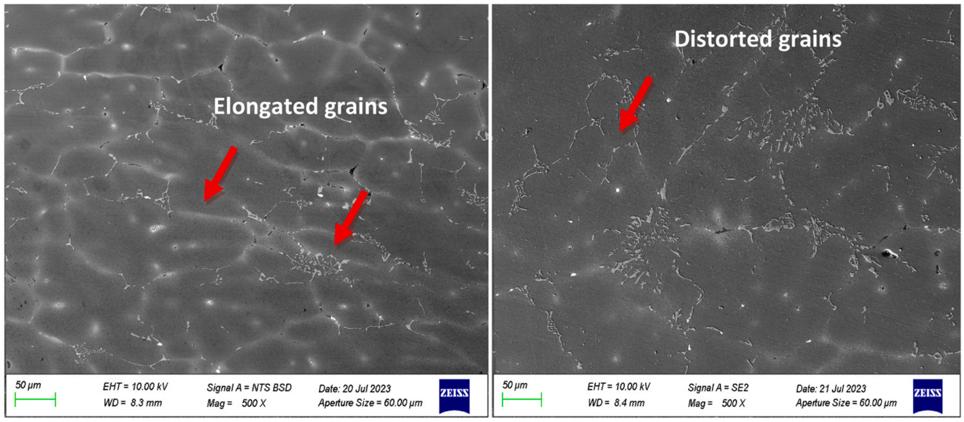

(a) (b)

Fig. 3. Representative SEM images of the instability regions of hot-compressed (0.5 global strain) Al-Zn/6 wt%SSp composites at (a) 250°C/0.01 s^{-1}, (b) 250°C/1.0 s^{-1}.

formation. In Fig. 5, which show the post deformation microstructure for processing at 350 °C/1 s^{-1}, new grain reorientation with equiaxed grains is visible. This corresponds with what is observed from the processing map at which the optimum deformation temperature and strain rate were experienced.

3.3. Flow stress behavior

The strain-stress curves achieved from the hot deformation testing of Al-Zn/6 % martensitic stainless steel composite samples are presented in Fig. 6a–d. The flow stress characteristically increased with increased strain rate and reduced deformation temperature. The decline in dislocation mobility at lower deformation temperatures can be ascribed to the reduced thermal activation observed at lower temperatures [2,20]. Normally, as the strain rate increases, dislocation piles up, and multiplication takes place, which gives rise to increased dislocation concentration in the developed composites. When dislocation concentration increases, there is usually a restriction to dislocation movement, hence promoting the flow stress increase required to sustain plastic deformation [21–23].

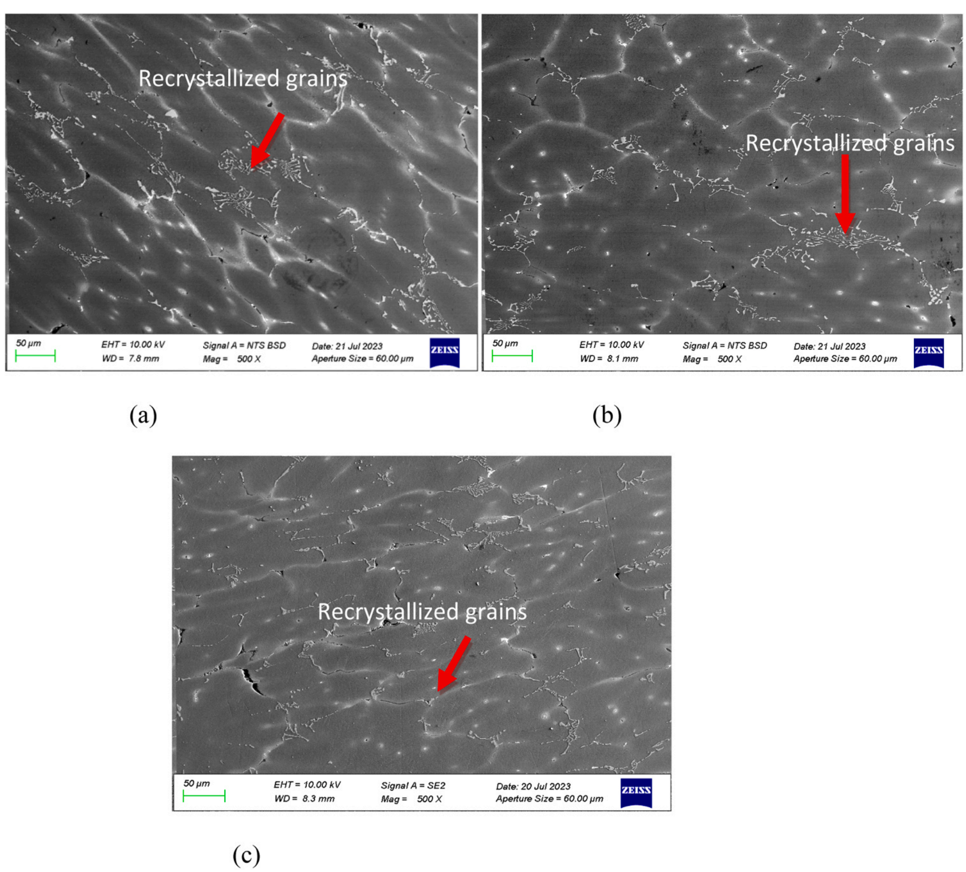

Fig. 4. SEM images of stable regions (a-c) of hot-compressed (0.5 global strain) Al-Zn/6 wt%SSp composites at (a) 300°C/0.01 s^{-1}, (b) 300°C/1.0 s^{-1}, and (c) 350°C/0.1 s^{-1}.

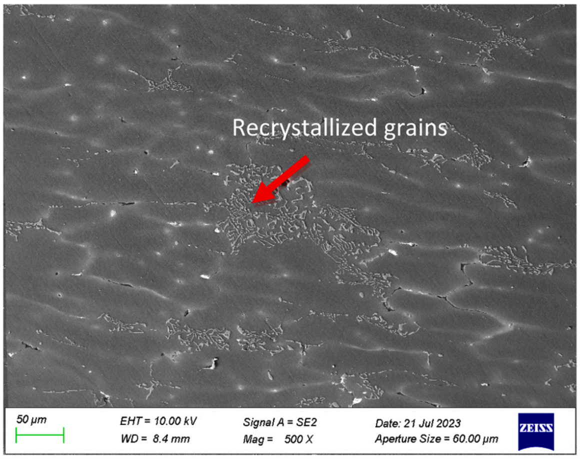

Fig. 5. SEM images of the optimum processing region of hot-compressed (0.5 global strain) Al-Zn/6 wt%SSp composite at 350°C/1.0 s^{-1}.

From all test parameters, there was an initial increase in the flow stress at a lower deformation strain rate as a result of the prevalence of work hardening. The most distinctive feature observed in the flow curves for the composite is the anomalous flow stress oscillations observed for samples hot deformed at a strain rate of 0.01 s^{-1}. In related studies by Alaneme *et al.* [1] and Babalola *et al.* [8], this phenomenon has been linked to the interactions between dislocations and the reinforcement particles which were mainly segregated along grain boundaries. The pinning effect of the reinforcement on dislocations is more noticeable at low strain rates, particularly where particle colonies are along grain boundaries. That is lower stresses are required to move the dislocations within the grain but at the boundaries, a high flow stress is required as a result of the pinning action of the strengthening particles and the grain boundary effect.

3.4. Constitutive modeling of the flow stress behavior of Al-Zn/6 % stainless steel composite

3.4.1. Constitutive analysis

The constitutive equation and associated activation energy are computed, respectively, to achieve a good insight into the flow behavior and deformation mechanisms of the developed composites [24]. The proposed Sellars and McTegart [25] proposed constitutive equations that centre on the hyperbolic sine law of Arrhenius type equation (Eq. 1) were utilized to characterize the hot workability response of Al-Zn/6 % martensitic stainless steel composite.

$$\dot{\varepsilon} = A[\sinh(\alpha\sigma)]^{n}\exp\left(-\frac{Q}{RT}\right) \tag{1}$$

$$\dot{\varepsilon} = 6.1000E+20[\sinh(0.011449 * 117.1017)]^{10.3627}\exp\left(-\frac{226.27152}{8.314 * 473.15}\right) \quad \dot{\varepsilon} = 0.01$$

where A, α, n, Q and R represents material constant, stress multiplier, stress exponent, hot work activation energy (kJ mol-1), and gas constant (8.314 $\frac{J}{mol\,K}$), respectively.

The value of the stress multiplier α is obtained using Eq. 2, where n' and β are derived from the slopes of the curves of Eq. 3 and Eq. 4 respectively.

The parameter β represent a constant parameter, σ is the peak stress, while the power law at low stresses is used to determine the constant n' [26].

$$\alpha = \frac{\beta}{n'} \tag{2}$$

where

$$n' = \frac{\partial \ln\dot{\varepsilon}}{\partial \ln\sigma_p} \tag{3}$$

$$\beta = \frac{\partial \ln\dot{\varepsilon}}{\partial \sigma_p} \tag{4}$$

Bambach *et al.* [27] showed that the partial differentiation of Eq. 1 at constant temperature gives

$$\frac{1}{n} = \left[\frac{\partial \ln[\sinh(\alpha\sigma_p))}{\partial \ln\dot{\varepsilon}}\right]_T \tag{5}$$

Similarly, the partial differentiation at a constant strain rate gives

$$Q = Rn\left[\frac{\partial \ln[\sinh(\alpha\sigma_p)]}{\partial\left(\frac{1}{T}\right)}\right]_{\dot{\varepsilon}} = Rnk \tag{6}$$

Insight on the effect of deformation temperature, strain rate and strain on the deformation characteristics of metallic materials, can be provided using the Zener-Hollomon parameter, Z expressed in Eq. 7:

$$Z = \dot{\varepsilon}\exp\left[\frac{Q}{RT}\right] = f(\sigma) = A[\sinh(\alpha\sigma)]^{n} \tag{7}$$

The natural log of Eq. 7 gives

$$\ln Z = \ln A + n\ln[\sinh(\alpha\sigma)] \tag{8}$$

Therefore, n′, β, α, n, k, Q, and lnA were found by linear regression of Eqs. 5 to 10 using the peak and steady-state values given in Table 2.

By taking the natural logarithm of the hyperbolic-sine law (Eq. 3) and solving for σ, the general equation for flow stress σ as a function of Z can be derived as shown in Eq. 9.

$$\sigma = \frac{1}{\alpha}\ln\left\{\left(\frac{Z}{A}\right)^{\frac{1}{n}} + \left[\left(\frac{Z}{A}\right)^{\frac{2}{n}} + 1\right]^{\frac{1}{2}}\right\} \tag{9}$$

Therefore, by using the material constants values from Eq. 2, the flow stress can be determined using Eq. 10:

$$\dot{\varepsilon} = 6.1000E+20[\sinh(0.011449\sigma)]^{10.3627}\exp\left(-\frac{226.27152}{RT}\right) \tag{10}$$

Then, from Eq. 10, the flow stress dependence on the deformation parameters ($\dot{\varepsilon}, T$) can therefore be determined using Eq. 11:

$$\sigma = 87.34387\ln\left\{\left(\frac{Z}{6.1000E+20}\right)^{0.0965} + \left[\left(\frac{Z}{6.1000E+20}\right)^{0.19299} + 1\right]^{\frac{1}{2}}\right\} \tag{11}$$

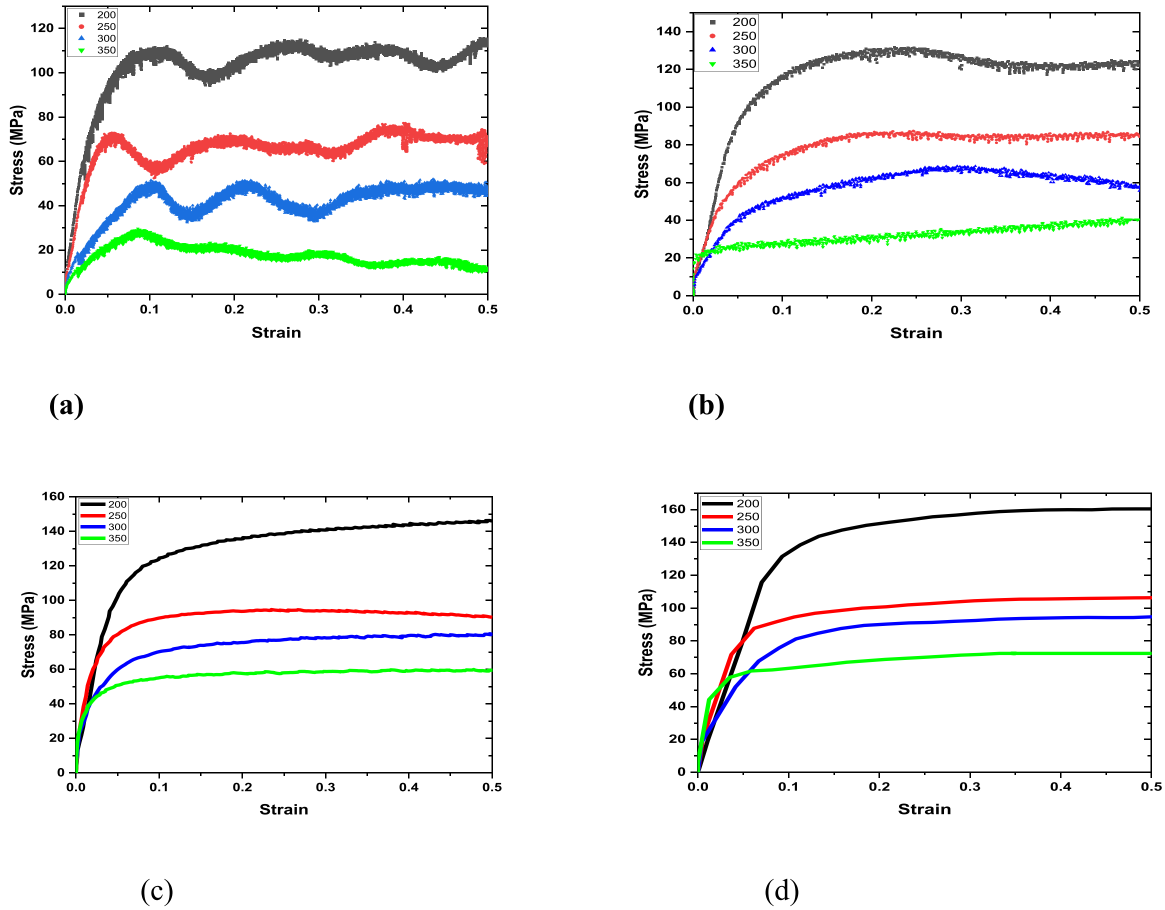

Fig. 6. Stress-Strain curves for (a)Al-Zn/6 %SS at 0.01 s^{-1}, (b) Al-Zn/6 %SS at 0.1 s^{-1}, (c) Al-Zn/6 %SS at 1.0 s^{-1}, and (d) Al-Zn/6 %SS at 10.0 s^{-1}.

Table 2
Peak stress (MPa) and steady state stress obtained from flow stress- strain curves of Al-Zn/6 %SS composite.

Peak Stress (σ_p, MPa) obtained at the test temperatures (°C)				
Strain rate (s^{-1})	200	250	300	350
0.01	117.1017	77.3227	52.0510	20.7833
0.1	131.7604	87.4309	68.7014	41.4277
1	146.3004	94.7010	80.7165	59.9584
10	160.4361	106.3551	94.7569	72.3990

3.4.2. *Activation energy for the hot worked composite*

Activation energy pertains to the capacity of materials to withstand deformation and the energy required to facilitate the distribution of dislocations, specifically in the context of hot working [21,28,29]. Multiple research [1,8,9] have proposed the processes that govern the deformation process using activation energy value. In addition, this methodology has been utilized to advance constitutive correlations to predict flow stress [30,31]. The Al-Zn/6 %SSp composite activation energy is assessed using the Arrhenius hyperbolic-sine equation. The selection of this equation is based on its simplicity and its capacity to effectively address stress circumstances of varying magnitudes. The ideal Q value is the material constant, which is determined by the microstructure and chemical composition of the composite that is formed. Typically, the hyperbolic law of the Arrhenius-type equation is utilized for its determination [32]. To calculate the activation energy, it is necessary to acquire constitutive constants like β, α,n, and lnA from the equation. The constants in question are derived by the process of fitting calculated data from the rearranged hyperbolic-sine equations, as described in Eqs. 5–6. The several graphs illustrating the derivation of each constitutive constant are depicted in Fig. 7a–e. Table 3 presents a comparative analysis of the activation energy derived from the present investigation to existing literature. The hot-worked Al-Zn composite exhibited an activation energy of 226.27 kJ/mol, which was 58 % greater than that of self-diffusion of aluminum (42 kJ/mol). This observation indicates that dynamic recrystallization is more prevalent than dynamic recovery in the state of deformation. This has been demonstrated by numerous researchers that have worked on the hot deformation characteristics of aluminum and its alloy [33–37]. Furthermore, the observed characteristics in the microstructure of the distorted samples provided additional support for this assertion. Therefore, based on the activation energy determined in this research study, it can be deduced that DRX is the primary flow deformation mechanism. The composite's stress exponent (n) value (10.327) surpassed 5, suggesting that work hardening is more prevalent than dynamic recrystallization. However, the post-deformation microstructures did not provide support for this assertion.

The values of the material constants obtained are summarized in Table 4.

The flow stress was calculated with the constitutive constants listed in Table 4. Fig. 8 shows from the plots of the measured and calculated stresses that a correlation coefficient (R^2) value of 0.97 was obtained for the composite material. This demonstrates the accuracy of the determined constitutive equation in precisely anticipating the test findings, confirming its ability to effectively forecast the hot deformation stress data of the Al-Zn/6 %SSp composite.

3.5. *Processing map*

To establish safe hot-work processing conditions for metallic mate-

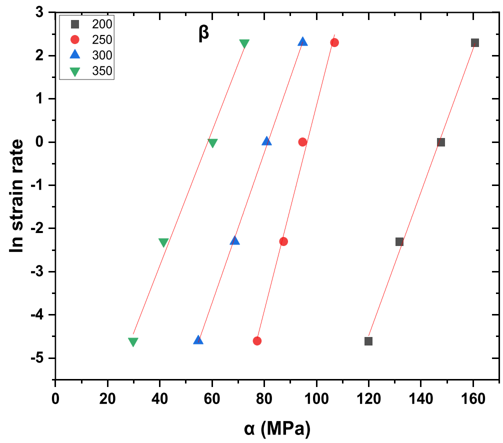

(a)

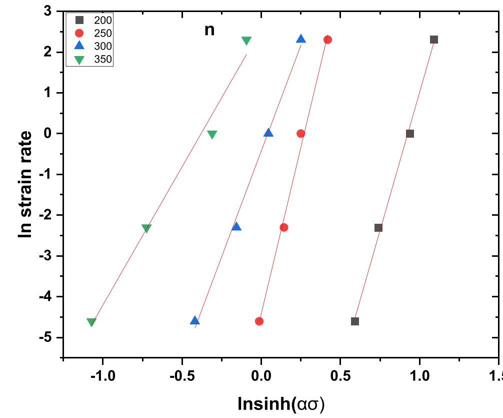

(b)

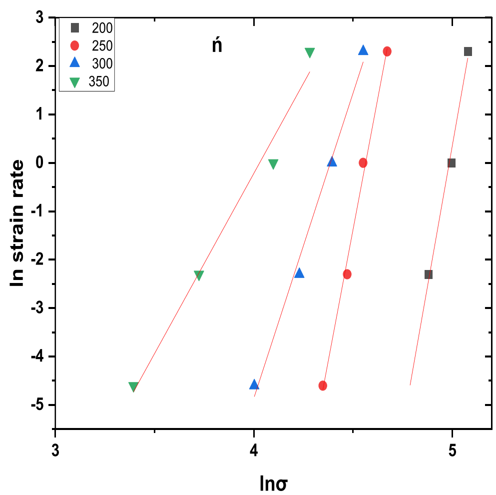

(c)

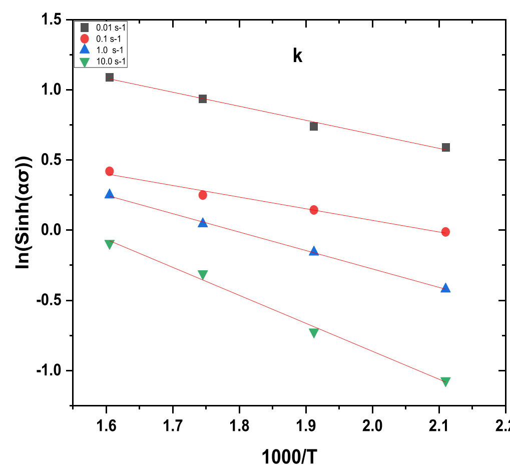

(d)

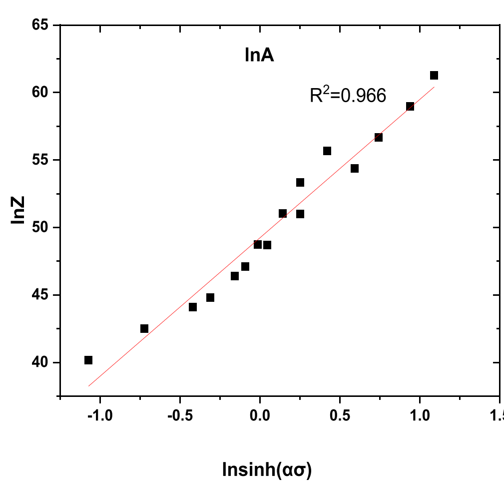

(e)

Fig. 7. a-e: materials constants deriving plots for the composite.

Table 3
Activation energy and hot-work process conditions of some aluminum alloys and composites.

S/n	Material System	Activation Energy (Kj/mol)	Deformation Processing Parameters	References
1.	Al-Zn/6 % martensitic Stainless Steel particles	226.27	200–350^0 C (0.01–10 S^{-1})	This work
2.	Al-Zn	155	200–350^0 C (0.01–10 S^{-1})	[18]
3.	Al-Zn/6 %Cu	179	200–350^0 C (0.01–10 S^{-1})	[18]
4.	Al-Zn/8 %Si	113	200–350^0 C (0.01–10 S^{-1})	[18]
5.	6063Al/6 % Ni particles	151	200–400^{0}C (0.01–10.0 S^{-1})	[2]
6.	6063 Al/6 % steel particles	168	200–400^{0}C (0.01–10.0 S^{-1})	[2]
7.	Al/8 % bamboo leaf ash-SiC	290.5	300–400^0 C (0.01–1.0 S^{-1})	[2]
8.	AA7075/Al2 O_3	289	350–500 °C (0.001–1.0 S^{-1})	[39]
9.	6061Al/20 % SiC	246	300–500 °C (0.001–1.0 S^{-1})	[35]
10.	6×82 Aluminium alloy	224.738	300–500^0 C (0.01–10 S^{-1})	[40]

rials, a processing map is normally employed [41]. A dynamic material model is commonly employed to develop the processing map of a material system [10]. The model regarded the material being deformed as a power dissipater. The entire power is divided into two components: power produced by increased temperature (due to plastic deformation) and dissipated power by structural changes like (DRX and DRV). Dynamic materials model (DMM) [10] was used to conduct an in-depth investigation on the hot compression of the Al-Zn/6 wt%SSp Composite. This is stated as efficiency of power dissipation (η) specified by Eq. 12:

$$\eta = \frac{J}{Jmax} = \frac{2m}{m+1} \tag{12}$$

Where η, J, and m stand for strain rate sensitivity, power dissipation efficiency through microstructural evolution, and coefficient of power dissipation efficiency, respectively. Eqs. 13 and 14 describe the dimensionless parameter ξ, (ε) as the instability criterion, which is used to establish the temperature and strain rate domains where there is flow instability.

$$\xi(\varepsilon) = m < 0 \tag{13}$$

Park and Kim, [42] state that.

$$\xi(\dot{\varepsilon}) = \frac{2m}{\eta} - 1 < 0 \tag{14}$$

where ξ ($\dot{\varepsilon}$), m, and η represents the instability parameter, strain rate sensitivity, and power dissipation efficiency, respectively.

The power efficiency, instability, and processing maps of the Al-Zn/6 %SSp under varied deformation conditions are presented in Fig. 9a-e. It is known from the literature that metal alloys with high power dissipation efficiency values are amenable to good hot workability during plastic deformation as the power input is effectively utilized by microstructural evolution via mechanisms of DRV, DRX, and phase transformation. Conversely, lower power dissipation efficiency values suggest poor workability, and the microstructures are usually characterized by defects such as inhomogeneity and porosity [18]. The contour map in Fig. 9a–b depicts the regions with the highest power dissipation efficiency (%) values (red-shaded region), which denotes the optimum safe processing region. This region corresponds with the microstructural features of the compressed samples that revealed recrystallized grains, while the regions with the lowest power dissipation efficiency values (blue shaded region) denote the instability region characterized with shear bands and cracks. These regions have to be avoided while processing the composite.

From Fig. 9c–d, the instability map shows no instability region because the instability criteria have positive values. It therefore denotes that flow instability did not occur at peak stress in the compressed samples. The Red Cross portion as shown in the processing map (Fig. 9e) represents the optimum processing region. At 0.5 strain, the instability domains take place at 200—270°C/0.01–10 s^{-1} and this parameter should be avoided while processing this composite. It has been observed that regions possessing high power efficiency and positive ξ values provide the optimum conditions for hot working characterized with defect-free microstructures facilitated by DRX [38,43], in this case when the composite is processed at 280–340°C/0.01–10 s^{-1}.

4. Conclusion

This study evaluated the hot deformation characteristics of an Al-Zn/6 wt% martensitic stainless steel particles-based composite. The following results were obtained:

- The Al-Zn/6 %SSp composite exhibited positive strain rate sensitivity characterized by flow stress increase with increase in strain rate and decrease in temperature.
- The constitutive equation from the hot-worked Al-Zn/6 %SSp composite resulted in an estimated activation energy of 226.27 kJ/mol, which was 58 % more than that for the self-diffusion of aluminum alloy (142 kJ/mol). These findings suggest dynamic recrystallization

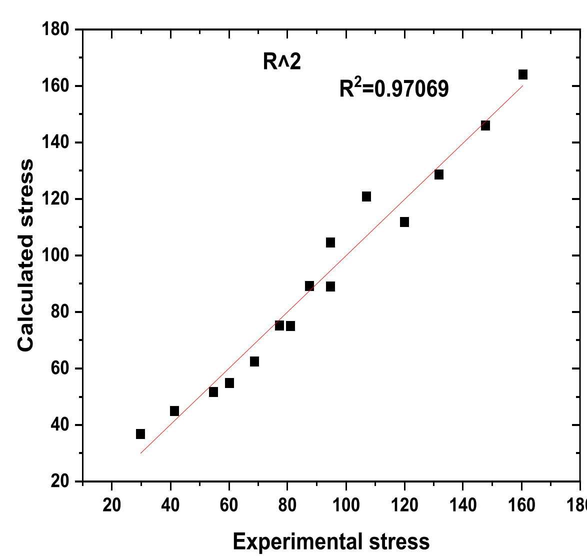

Fig. 8. Showing relationship between calculated stress and experimental stress data.

Table 4
Material constants for constitutive modelling of Al-Zn/6 %SS composite.

n'	β	α (MPa^{-1})	n	k	Q ($kJmol^{-1}$)	lnA	A
15.7217	0.18	0.011449	10.3627	2.626	226.27152	47.86	6.10006E+20

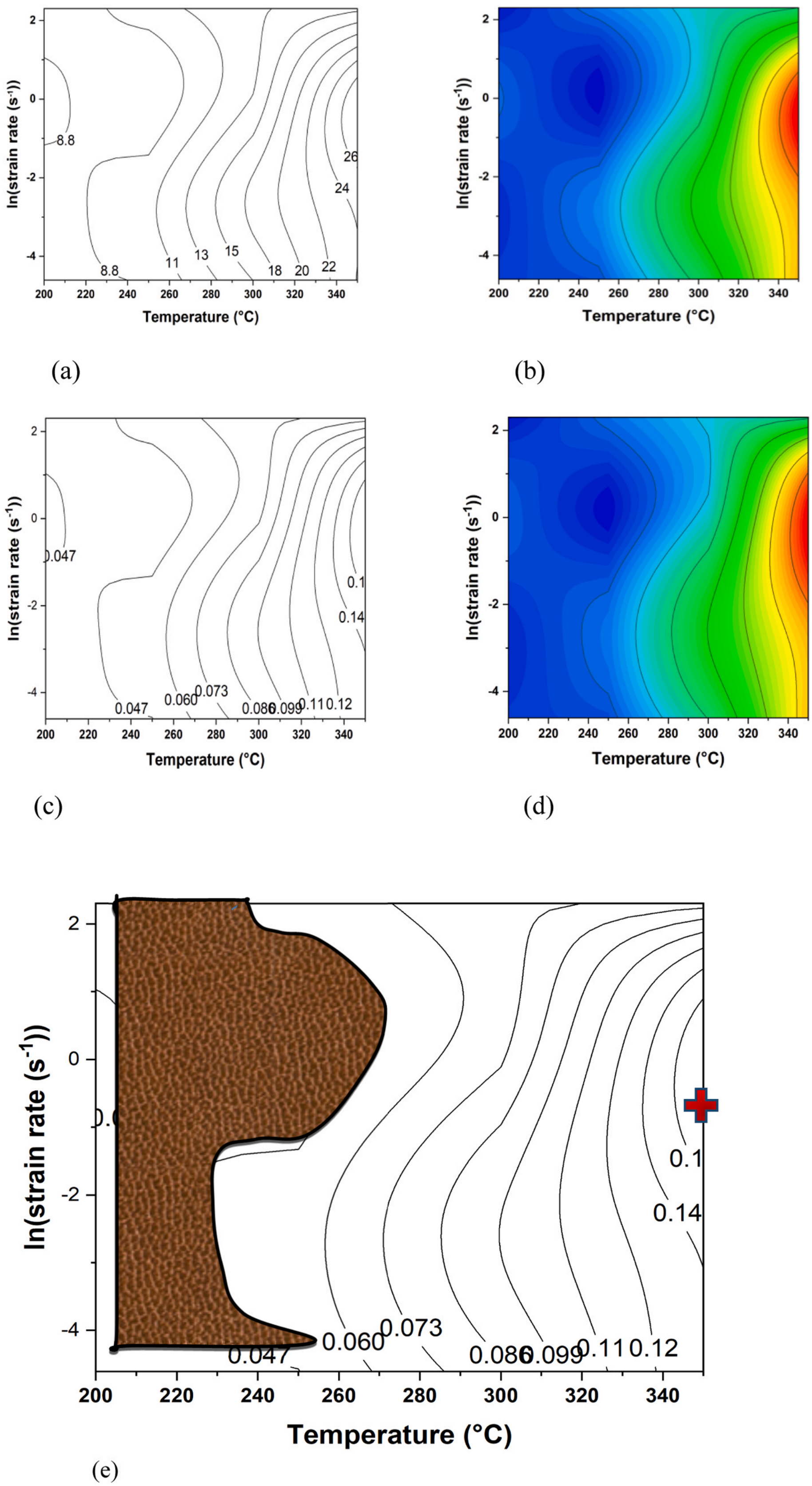

Fig. 9. Power efficiency maps (a and b) for Al-Zn/6 % Martensitic Stainless Steel, instability maps (c and d) for Al-Zn/6 % Martensitic Stainless Steel, and processing map (e) for Al-Zn/6 % Martensitic Stainless Steel.

(DRX) as the dominant deformation mechanism, as confirmed from the microstructures of the hot worked samples.

- Work hardening was predicted to dominate the deformation process by the stress exponent *(n)* value of 10.36 (which exceeded 5), but this was not supported by the microstructures.
- Comparing the linear fitting of calculated flow stress data with the estimated flow stress yielded a correlation coefficient (R^2) of approximately 0.97. This observation demonstrates an effective relationship involving the calculated stress with the computed stress value for the composite material that was fabricated.
- Based on the processing map analysis, the instability regime occurs at 200—270 °C/0.01–10 s^{-1}. The stable domain established was at 280–340°C/0.01–10 s^{-1} which is most suitable for achieving the best microstructural conditions for enhanced service performance.

CRediT authorship contribution statement

Theo Joshua: Writing – original draft, Methodology, Investigation, Data curation. **Kenneth Kanayo Alaneme:** Writing – review & editing, Writing – original draft, Validation, Supervision, Project administration, Funding acquisition, Data curation, Conceptualization. **Michael Bodunrin:** Supervision, Methodology. **Sodiq Kareem:** Writing – review & editing, Formal analysis.

Acknowledgements

The authors wish to appreciate the support of their respective institutions, and the National Research Foundation (NRF), South Africa through the Grant No: 138062, administered by The University of Johannesburg, South Africa.

References

[1] K.K. Alaneme, S.A. Babalola, M.O. Bodunrin, L.H. Chown, E.A. Okotete, N. B. Maledi, Hot deformation of nickel particles reinforced aluminium based composites: flow behaviour, microstructural evolution and processing map analyses, Mater. Res. Express 8 (2021) 1–10.
[2] K.K. Alaneme, S.A. Babalola, L.H. Chown, M.O. Bodunrin, Hot deformation behaviour of bamboo leaf ash–silicon carbide hybrid reinforced aluminium based composite, Manuf. Rev. 7 (17) (2020) 1–14.
[3] G.Karthik Pandiyan, T. Prabaharan, Mechanical and Tribological characterization of stir cast AA6061 T6 – SiC composite Silicon, 12 (11) (2020), pp. 1-8.
[4] T.O. Joshua, K.K. Alaneme, M.O. Bodunrin, J. Omotoyinbo, Microstructure, mechanical behaviour and damping characterisitics of Al-Zn composites reinforced with martensitic stainless steel (410L) and silicon carbide, Int. J. Lightweight Mater. Manuf. Volume 5 (Issue 3) (2022) 279–288.
[5] Y.C. Lin, M.S. Chen, J. Zhong, Mech. Res. Commun. (2008) 142–150.
[6] Z.Y. Huang, X.X. Zhang, B.L. Xiao, Z.Y. Ma, Hot deformation mechanisms and microstructure evolution of SiCp/2014Al composite, J. Alloys Compd. 722 (2017) 145–157.
[7] Y.C. Lin, X.M. Chen, Mater. Des. vol. 32 (2011) 1733–1759.
[8] S.A. Babalola, K.K. Alaneme, S.R. Oke, L.H. Chown, N.B. Maledi, M.O. Bodunrin, Hot compression behavior and microstructural evolution in aluminium based composites; an assessment of the role of reinforcements and deformation parameters, Manuf. Rev. 8 (2021) 6.
[9] M.O. Bodunrin, Flow stress prediction using hyperbolic sine Arrhenius constants optimized by simple generalized reduced gradient refinement, J. Mater. Resour. Technol. 9 (2) (2020) 2376–2386.
[10] Y. Prasad, K. Rao, S. Sasidhar, Hot Working Guide: A Compendium of Processing Maps, ASM International, Cleveland, OH, USA, 2015.
[11] G.Z. Quan, W.Q. Lv, Y.P. Mao, Y.W. Zhang, J. Zhou, Mater. Des. 50 (2013) 51–61.
[12] D.-X. Wen, Y.C. Lin, J. Chen, J. Deng, X.-M. Chen, J.-L. Zhang, M. He, Effects of initial aging time on processing map and microstructures of a nickel-based superalloy, Mater. Sci. Eng. A 620 (2015) 319–332.
[13] S. Jiang, Y. Wang, B. Yan, Y. Zhang, Hot workability of FeMnSiCrNi shape memory alloy based on processing map and martensitic transformation, J. Alloys Compd. 806 (2019) 1153–1165.
[14] K.K. Alaneme, S.A. Babalola, M.O. Bodunrin, On the prediction of hot deformation mechanisms and workability in AL6063/Nip and AL6063/steelp composites using hyperbolic-sine constitutive equation, Mater. Today Proc. 38 (2021) 942–948.
[15] Tao Wei, Yadong Wang, Zhenghua Tang, Sufen Xiao, The constitutive modeling and processing map of homogenized Al-Mg-Si-Cu-Zn alloy, Mater. Today Commun. Volume 27 (2021) 102471.
[16] Garrison Jr, W.M., & Amuda, M.O.H. (2017). Stainless Steels: Martensitic.
[17] Y. Murakami, Martensitic stainless steels, Metal Fatigue (Second Edition), Effects of Small Defects and Nonmetallic Inclusions, 2019, 431-451.
[18] K.K. Alaneme, S.A. Kareem, M.O. Bodunrin, Hyperbolic – Sine constitutive model determine hot deformation mechanisms and workability response of Al-Zn/Cu and Al-Zn/SiC based composites, Results Eng. 19 (2023) 101255.
[19] C. Shuan, T. Jie, L. Haibo, W. Yu, Z. Hui, Mater. Sci. Eng. A 697 (2017) 194–202.
[20] Y. Yang, Z. Zhang, X. Zhang, processing map of Al_2O_3 particulate reinforced Al alloy matrix composite, Mater. Sci. Eng. Adv. 558 (2012) 112–118.
[21] S. Chen, J. Teng, H. Luo, Y. Wang, H. Zhang, Hot deformation characteristics and mechanism of PM 8009Al/SiC particle reinforced composites, Mater. Sci. Eng. Adv. 697 (2017) 194–202.
[22] S. Hao, et al., Hot deformation behaviors of 35%SiCp/2024Al metal matrix composites. Trans. Nonferrous Metall. Soc. China 24 (2014) 2468–2474.
[23] L. Saravanan, T. Senthilvelan, Investigations on the hot workability characteristics and deformation mechanisms of aluminium alloy-Al_2O_3 nanocomposite, Mater. Des. 79 (2015) 6–14.
[24] A. He, X.Y. Yang, G.L. Xie, X.T. Wang, H.L. Zhang, Finite element analysis and experimental study of microstructure evolution of nitrogen alloyed ultralow carbon stainless steel during hot deformation, Mater. High. Temp. 32 (5) (2015) 502–511.
[25] C.M. Sellars, W.J. McTegart, On the mechanism of hot deformation, Mem. Sci. Rev. Met. 63 (1966) 731–746.
[26] S. Jiang, Y. Wang, B. Yan, Y. Zhang, Hot workability of FeMnSiCrNi shape memory alloy based on processing map and martensitic transformation, J. Alloys Compd. 806 (2019) 1153–1165.
[27] M. Bambach, A. Emdadi, I. Sizova1, U. Hecht, F. Pyczak, Isothermal forging of titanium aluminides without beta-phase — using non-equilibrium phases produced by spark plasma sintering for improved hot working behavior, Intermetallics 101 (2018) (2018) 44–55.
[28] M.J. Luton, C.M. Sellars, Dynamic recrystallization in nickel and nickel-iron alloys during high temperature deformation, Acta Metall. 17 (1969) 1033–1043.
[29] D.F. Li, D.Z. Zhang, S.D. Liu, Z.J. Shan, X.M. Zhang, W.A.N.G. Qin, S.Q. Han, Dynamic recrystallization behavior of 7085 aluminum alloy during hot deformation, Trans. Nonferrous Met. Soc. China 26 (6) (2016) 1491–1497.
[30] J. Cai, K. Wang, P. Zhai, F. Li, J. Yang, A modified Johnson – Cook constitution equation to predict hot deformation behaviour of Ti-6Al-4V alloy, J. Mater. Eng. Perform. 24 (2015) 32–44.
[31] N. Tahreen, D.F. Zhang, F.S. Pan, X.Q. Jiang, D.Y. Li, D.L. Chen, Hot deformation and processing map of an as-extruded Mg–Zn–Mn–Y alloy containing I and W phases. Mater. Des. 87 (2015) 245–255.
[32] C.M. Sellars, W.M. Tegart, Hot workability, Int. Metall. Rev. 17 (1972) 1–24.
[33] G.E. Dieter, H.A. Kuhn, S.L. Semiatin, Handbook of workability and process design, ASM International, 2003.
[34] H. Shi, A. Mclaren, A. Sellars, C.M.R. Shahani, R. Bolingbroke, Constitutive equations for high temperature flow stress of aluminium alloys, Mater. Sci. Technol. 13 (1997) 210–216.
[35] X. Wenchen, J. Xueze, X. Wendeng, Z. Xiangqian, S. Debin, Study on hot deformation behavior and workability of squeeze-cast 20 vol% SiCw/6061Al composites using processing map, Mater. Charact. 135 (2018) 154–166.
[36] H.J. Mcqueen, S. Yue, N.D. Ryan, E. Fry, J. Mater. Process. Technol. 53 (1995) 293–310.
[37] C.C. Nwaeju, F.O. Edoziuno, A.A. Adediran, T.J. Tuaweri, M.S. Kumar, Grain characteristics and mechanical properties of as-cast Cu-10% Al alloy: effects of alloying additions, Results Eng. 12 (2021) 100295 (Article).
[38] S.S. Zhou, K.K. Deng, J.C. Li, K.B. Nie, F.J. Xu, H.F. Zhou, J.F. Fan, Hot deformation behavior and workability characteristics of bimodal size SiCp/AZ91 magnesium matrix composite with processing map, Mater. Des. 64 (2014) 177–184.
[39] Hr Ezatpour, A. Chaichi, S.A. Sajjadi, The effect of Al_2O_3- nanoparticles as the reinforcement additive on the hot deformation behavior of 7075 aluminum alloy, Mater. Des. 88 (2015) 1049–1056.
[40] X. Kai, C. Chen, X. Sun, C. Wang, Y. Zhao, Hot deformation behavior and optimization of processing parameters of a typical high-strength Al–Mg–Si alloy, Mater. Des. 90 (2016) 1151–1158.
[41] M.H. Wang, L. Huang, M.L. Chen, Y.L. Wang, Processing map and hot working mechanisms of Cu-Ag alloy in hot compression process, J. Cent. South Univ. vol. 22 (3) (2015) 821–828.
[42] S.Y. Park, W.J. Kim, Difference in the hot compressive behavior and processing maps between the As-cast and homogenized Al-Zn-Mg-Cu (7075) alloys, J. Mater. Sci. Technol. 32 (2016) 660–670.
[43] W. Xu, X. Jin, W. Xiong, X. Zeng, Shan, Study on hot deformation behavior and workability of squeeze-cast 20 vol%SiCw/6061Al composites using processing map, Mater. Charact. 135 (2018) 154–166.